DISCRETE AND CONTINUOUS
DYNAMICAL SYSTEMS SERIES B
Volume **24**, Number **9**, September **2019**

doi:10.3934/dcdsb.2019041

pp. **4983–5001**

KRYLOV IMPLICIT INTEGRATION FACTOR WENO METHOD FOR SIR MODEL WITH DIRECTED DIFFUSION

Ruijun Zhao*

Department of Mathematics and Statistics
Minnesota State University, Mankato
Mankato, MN 56001, USA

Yong-Tao Zhang

Department of Applied and Computational Mathematics and Statistics
University of Notre Dame
Notre Dame, IN 46556, USA

Shanqin Chen

Department of Mathematical Sciences
Indiana University South Bend
South Bend, IN 46615, USA

(Communicated by Qing Nie)

Abstract. SIR models with directed diffusions are important in describing the population movement. However, efficient numerical simulations of such systems of fully nonlinear second order partial differential equations (PDEs) are challenging. They are often mixed type PDEs with ill-posed or degenerate components. The solutions may develop singularities along with time evolution. Stiffness due to nonlinear diffusions in the system gives strict constraints in time step sizes for numerical methods. In this paper, we design efficient Krylov implicit integration factor (IIF) Weighted Essentially Non-Oscillatory (WENO) method to solve SIR models with directed diffusions. Numerical experiments are performed to show the good accuracy and stability of the method. Singularities in the solutions are resolved stably and sharply by the WENO approximations in the scheme. Unlike a usual implicit method for solving stiff nonlinear PDEs, the Krylov IIF WENO method avoids solving large coupled nonlinear algebraic systems at every time step. Large time step size computations are achieved for solving the fully nonlinear second-order PDEs, namely, the time step size is proportional to the spatial grid size as that for solving a pure hyperbolic PDE. Two biologically interesting cases are simulated by the developed scheme to study the finite-time blow-up time and location or discontinuity locations in the solution of the SIR model.

1. **Introduction.** There have been a lot of mathematical models studying the diffusion of biological populations since 1970s. These models can roughly be classified into two groups: One is based on the assumption that dispersal is due to a random motion of individuals [27, 24, 1]; the other is based on the assumption that

2010 *Mathematics Subject Classification.* Primary: 92D30, 65M06; Secondary: 92-08.

Key words and phrases. SIR model, directed diffusion, Krylov implicit integration factor methods, weighted essentially non-oscillatory schemes.

The second author is supported by NSF grant DMS-1620108.

* Corresponding author: Ruijun Zhao.

dispersal is a response of population pressure, which is often called the directed spatial diffusion [9, 22, 15, 5, 4, 3, 16, 18]. In the biological world, some species have been observed migrating to avoid crowding rather than random motion. As early as recorded in 1971, arctic ground squirrels migrate from densely populated areas into sparsely populated areas, even when the latter provide a less favorable habitat [6, 9]. In 1983, MacCamy [15] proposed a model with directed spatial diffusion to avoid crowd in the setting of studying epidemic diseases. In this model, it is assumed that infectives and removed do not move while susceptibles move away from concentrations of infectives. Milner et al. [16, 17, 18] extended the model to a more general case: not only do each individual move away from crowd, but also susceptibles moves away from concentrations of infectives. Let $S(\vec{x},t)$, $I(\vec{x},t)$, and $R(\vec{x},t)$ denote the density functions of susceptible, infected, and recovered human population at location $\vec{x}$ and time t. The model in [18] is formulated as

$$\left\{\begin{array}{rcl} S_t &=& k_1\nabla\cdot(S\nabla P)+k_2\nabla\cdot(S\nabla I)-\alpha SI,\\ I_t &=& k_1\nabla\cdot(I\nabla P)+\alpha SI-\gamma I,\\ R_t &=& k_1\nabla\cdot(R\nabla P)+\gamma I, \end{array}\right. \tag{1}$$

for $\vec{x}\in\Omega\subset\mathbb{R}^n$ and $t\in(0,T)$ for some $T>0$, where $P(\vec{x},t)=S(\vec{x},t)+I(\vec{x},t)+R(\vec{x},t)$ is the density function of total population; $\alpha>0$ and $\gamma>0$ are epidemiological parameters and $k_1\geq 0$ and $k_2\geq 0$ are diffusion parameters. The system is completed with nonnegative initial condition

$$S(\vec{x},0)=S_0(\vec{x}), I(\vec{x},0)=I_0(\vec{x}), R(\vec{x},0)=R_0(\vec{x})$$

and no-flux boundary conditions

$$\frac{\partial S}{\partial\vec{x}}(\vec{x},t)=\frac{\partial I}{\partial\vec{x}}(\vec{x},t)=\frac{\partial R}{\partial\vec{x}}(\vec{x},t)=0 \text{ on } \partial\Omega.$$

The density-dependent cross-diffusion term $\nabla\cdot(S\nabla I)$ has been used to model disease avoidence for studying pattern formation [2, 28].

The mathematical models with random diffusion can be classified into diffusion partial differential equations hence the models are well-posed [27, 1]. However, most models with cross-diffusion are degenerate, sometimes even ill-posed [3]. For the model 1, if we write the right-hand side of Eq 1 as a matrix times the column vector of the higher-order terms plus a term involving derivatives of lower order, then the three eigenvalues of the matrix are

$$\lambda_1=0, \lambda_{2,3}=\frac{k_1(S+I+R)\pm\sqrt{4k_1k_2SI+k_1^2(S+I+R)^2}}{2}.$$

If $k_1>0$ and $k_2=0$, then we have two zero eigenvalues and one positive eigenvalue; If $k_1=0$ and $k_2>0$, then we have three zero eigenvalues; If $k_1>0$ and $k_2>0$, then we have one positive, one negative, and one zero eigenvalue. Li and Yip proved that the Eq. 1 is ill-posed when $k_1>0$ and $k_2>0$ in terms of long-term behavior [12]. The well-posedness of Eq. 1 is still an open problem. But we conjecture that the Eq. 1 has a unique solution for some time $T>0$.

There are numerous efficient numerical methods for solving some mathematical models with spatial cross-diffusions [2, 25, 7]. However, the degeneracy of Eq. 1 poses a challenge in simulating it. Zhao and Milner [18] proposed a split Runge-Kutta discontinuous Galerkin method to solve Eq. 1. However, the method has only first-order accuracy. In the special case $k_1=0$ and $k_2>0$, Eq. 1 might have a finite-time blow-up solution or there might develop a shock solution [17, 18].

High order WENO schemes are a class of efficient numerical methods to stably resolve singularities while maintaining high order accuracy in smooth regions of the solution [23, 30]. It is natural to apply WENO schemes in solving this challenging model here. To perform efficient numerical simulations for this time dependent PDE system, an effective temporal numerical scheme is needed. The difficulty here is due to the stiffness of the system caused by nonlinear diffusion terms, since traditional implicit methods for solving stiff systems need to solve a large coupled nonlinear algebraic system at every time step, and often advanced preconditioning techniques have to be developed to improve the convergence of nonlinear algebraic solver. To avoid solving large nonlinear algebraic system at every time step and achieve large time step sizes, an efficient approach is the implicit integration factor (IIF) methods. IIF methods are a class of integration factor type time discretization methods, which perform the time evolution of stiff operators via evaluation of exponential functions of the corresponding matrices. IIF methods were originally developed in [19] for solving stiff one dimensional reaction-diffusion systems. A nice property of the methods is that the implicit terms are free of the exponential operation. The size of the nonlinear algebraic system resulting from the implicit treatment is independent of the number of spatial grid points. It only depends on the number of the original PDEs in the mathematical model itself, and no large nonlinear algebraic system needs to be solved at every time step. To overcome the difficulty in applying integration factor type methods to high dimensional problems, two different approaches were developed, i.e., the compact IIF methods [20, 26] and the Krylov IIF methods [8, 13]. In [11], high order Krylov IIF WENO schemes were developed to efficiently solve fully nonlinear stiff advection-diffusion-reaction equations.

In this paper, we design the Krylov IIF WENO method to solve the SIR model Eq. 1. We focus on the two spatial dimension case in this paper. Denote $\vec{X} = [S, I, R]^T$, then Eq. 1 can be written in a matrix form

$$\vec{X}_t + \vec{H}(\vec{X}_x, \vec{X}_y) = A(\vec{X})(\vec{X}_{xx} + \vec{X}_{yy}) + C(\vec{X}), \tag{2}$$

where

$$A(\vec{X}) = \begin{pmatrix} k_1 S & (k_1+k_2)S & k_1 S \\ k_1 I & k_1 I & k_1 I \\ k_1 R & k_1 R & k_1 R \end{pmatrix}, C(\vec{X}) = \begin{pmatrix} -\alpha SI \\ \alpha SI - \gamma I \\ \gamma I \end{pmatrix},$$

$$\begin{aligned} \vec{H}[\vec{X}_x, \vec{X}_y] &= \begin{pmatrix} -k_1 S_x(S_x + I_x + R_x) - k_2 S_x I_x \\ -k_1 I_x(S_x + I_x + R_x) \\ -k_1 R_x(S_x + I_x + R_x) \end{pmatrix} \\ &+ \begin{pmatrix} -k_1 S_y(S_y + I_y + R_y) - k_2 S_y I_y \\ -k_1 I_y(S_y + I_y + R_y) \\ -k_1 R_y(S_y + I_y + R_y) \end{pmatrix}. \end{aligned}$$

By forming the system Eq. 2 from the original model Eq. 1, the non-diffusion term $\vec{H}(\vec{X}_x, \vec{X}_y)$ is separated from diffusion terms. It has a form of Hamilton-Jacobi type operators, so high order WENO schemes for Hamilton-Jacobi equations (e.g., [21, 29]) can be naturally used to discretize $\vec{H}(\vec{X}_x, \vec{X}_y)$. Then the Krylov IIF method for fully nonlinear stiff advection-diffusion-reaction equations in [11] can be smoothly adopted to solve the Hamilton-Jacobi-diffusion-reaction system Eq. 2.

The organization of the paper is as follows. In Section 2 we will introduce the Krylov IIF WENO numerical scheme for the SIR model Eq. 2; In Section 3, we will

demonstrate the order of accuracy of the proposed numerical method using extended systems with known analytic solutions; In Section 4, we will numerically solve the SIR model Eq. 2 for biologically interesting cases using the proposed numerical scheme; In Section 5, we will give some remarks and discussions.

2. **The Krylov IIF WENO scheme for SIR model.** Let $\Omega = (a,b)\times(c,d)$. Consider a partition in space $a = x_0 < x_1 < x_2 < \cdots < x_{M-1} < x_M = b$, $c = y_0 < y_1 < y_2 < \cdots < y_{N-1} < y_N = d$, where $x_i = a + i\Delta x$, $y_j = c + j\Delta y$, for $i = 0,1,2,\ldots,M$, $j = 0,1,2,\ldots,N$, and $\Delta x = (b-a)/M$, $\Delta y = (d-c)/N$. Let $u_{i,j} \approx u(x_i, y_j, \cdot)$, for $u = S, I, R$, $i = 1,2,\ldots,M-1$, $j = 1,2,\ldots,N-1$. At the meshpoint (x_i, y_j), $i = 1,2,\ldots,M-1$, $j = 1,2,\ldots,N-1$, the diffusion terms are discretized using the second order central difference, i.e.,

$$(A\vec{X}_{xx})(x_i,y_j,\cdot) \approx \begin{pmatrix} k_1S_{i,j} & (k_1+k_2)S_{i,j} & k_1S_{i,j} \\ k_1I_{i,j} & k_1I_{i,j} & k_1I_{i,j} \\ k_1R_{i,j} & k_1R_{i,j} & k_1R_{i,j} \end{pmatrix} \begin{pmatrix} \dfrac{S_{i+1,j}-2S_{i,j}+S_{i-1,j}}{\Delta x^2} \\ \dfrac{I_{i+1,j}-2I_{i,j}+I_{i-1,j}}{\Delta x^2} \\ \dfrac{R_{i+1,j}-2R_{i,j}+R_{i-1,j}}{\Delta x^2} \end{pmatrix},$$

$$(A\vec{X}_{yy})(x_i,y_j,\cdot) \approx \begin{pmatrix} k_1S_{i,j} & (k_1+k_2)S_{i,j} & k_1S_{i,j} \\ k_1I_{i,j} & k_1I_{i,j} & k_1I_{i,j} \\ k_1R_{i,j} & k_1R_{i,j} & k_1R_{i,j} \end{pmatrix} \begin{pmatrix} \dfrac{S_{i,j+1}-2S_{i,j}+S_{i,j-1}}{\Delta y^2} \\ \dfrac{I_{i,j+1}-2I_{i,j}+I_{i,j-1}}{\Delta y^2} \\ \dfrac{R_{i,j+1}-2R_{i,j}+R_{i,j-1}}{\Delta y^2} \end{pmatrix}.$$

For discretizing the Hamilton-Jacobi term, we use the third order WENO scheme with Lax-Friedrichs flux [21, 31], i.e.,

$$\begin{aligned} \vec{H}(\vec{X}_x,\vec{X}_y)(x_i,y_j,\cdot) &\approx \hat{H}((\vec{X}_x)^-_{i,j},(\vec{X}_x)^+_{i,j},(\vec{X}_y)^-_{i,j},(\vec{X}_y)^+_{i,j}) \\ &= \vec{H}\left(\frac{(\vec{X}_x)^-_{i,j}+(\vec{X}_x)^+_{i,j}}{2},\frac{(\vec{X}_y)^-_{i,j}+(\vec{X}_y)^+_{i,j}}{2}\right) \\ &\quad -\frac{1}{2}\alpha_x((\vec{X}_x)^+_{i,j}-(\vec{X}_x)^-_{i,j}) - \frac{1}{2}\alpha_y((\vec{X}_y)^+_{i,j}-(\vec{X}_y)^-_{i,j}), \end{aligned}$$

where

$$\alpha_s = \max_{\substack{1\le i\le M-1\\ 1\le j\le N-1}} \max\left(\rho\left(\frac{\partial\vec{H}}{\partial\vec{X}_s}((\vec{X}_x)^+_{i,j},(\vec{X}_y)^+_{i,j})\right),\rho\left(\frac{\partial\vec{H}}{\partial\vec{X}_s}((\vec{X}_x)^-_{i,j},(\vec{X}_y)^-_{i,j})\right)\right), \tag{3}$$

for $s = x, y$. Here $\rho(\cdot)$ is the spectral radius operator. It is worth pointing out that $\frac{\partial\vec{H}}{\partial\vec{X}_x}$ and $\frac{\partial\vec{H}}{\partial\vec{X}_y}$ are 3 by 3 matrices, so the eigenvalues of them can be easily found analytically and spectral radius ρ can be computed efficiently. $(\vec{X}_x)^\pm_{i,j} = [(S_x)^\pm_{i,j},(I_x)^\pm_{i,j},(R_x)^\pm_{i,j}]^T$ and for $u = S, I, R$, a third order WENO approximation for u_x at the grid point (i,j) when the wind "blows" from the left to the right is

$$(u_x)^-_{i,j} = (1-w_-)\left(\frac{u_{i+1,j}-u_{i-1,j}}{2\Delta x}\right) + w_-\left(\frac{3u_{i,j}-4u_{i-1,j}+u_{i-2,j}}{2\Delta x}\right),$$

where

$$w_- = \frac{1}{1+2r_-^2}, \qquad r_- = \frac{\epsilon + (u_{i,j} - 2u_{i-1,j} + u_{i-2,j})^2}{\epsilon + (u_{i+1,j} - 2u_{i,j} + u_{i-1,j})^2};$$

on the other hand, the third order WENO approximation for u_x at the grid point (i, j) when the wind "blows" from the right to the left is

$$(u_x)^+_{i,j} = (1 - w_+)\left(\frac{u_{i+1,j} - u_{i-1,j}}{2\Delta x}\right) + w_+\left(\frac{-u_{i+2,j} + 4u_{i+1,j} - 3u_{i,j}}{2\Delta x}\right),$$

where

$$w_+ = \frac{1}{1+2r_+^2}, \qquad r_+ = \frac{\epsilon + (u_{i+2,j} - 2u_{i+1,j} + u_{i,j})^2}{\epsilon + (u_{i+1,j} - 2u_{i,j} + u_{i-1,j})^2}.$$

Similarly for approximations of derivatives in y-direction $(\vec{X}_y)^\pm_{i,j} = [(S_y)^\pm_{i,j}, (I_y)^\pm_{i,j}, (R_y)^\pm_{i,j}]^T$, third order WENO approximations are computed as following:

$$(u_y)^-_{i,j} = (1 - w_-)\left(\frac{u_{i,j+1} - u_{i,j-1}}{2\Delta y}\right) + w_-\left(\frac{3u_{i,j} - 4u_{i,j-1} + u_{i,j-2}}{2\Delta y}\right),$$

where

$$w_- = \frac{1}{1+2r_-^2}, \qquad r_- = \frac{\epsilon + (u_{i,j} - 2u_{i,j-1} + u_{i,j-2})^2}{\epsilon + (u_{i,j+1} - 2u_{i,j} + u_{i,j-1})^2};$$

$$(u_y)^+_{i,j} = (1 - w_+)\left(\frac{u_{i,j+1} - u_{i,j-1}}{2\Delta y}\right) + w_+\left(\frac{-u_{i,j+2} + 4u_{i,j+1} - 3u_{i,j}}{2\Delta y}\right),$$

where

$$w_+ = \frac{1}{1+2r_+^2}, \qquad r_+ = \frac{\epsilon + (u_{i,j+2} - 2u_{i,j+1} + u_{i,j})^2}{\epsilon + (u_{i,j+1} - 2u_{i,j} + u_{i,j-1})^2},$$

for $u = S, I, R$.

After the spatial discretizations, we consider the time discretization. Let the vector $\vec{U} = [S_{1,1}, I_{1,1}, R_{1,1}, \ldots, S_{M-1,1}, I_{M-1,1}, R_{M-1,1}, S_{1,2}, I_{1,2}, R_{1,2}, \ldots, S_{M-1,2}, I_{M-1,2}, R_{M-1,2}, \ldots, S_{1,N-1}, I_{1,N-1}, R_{1,N-1}, \ldots, S_{M-1,N-1}, I_{M-1,N-1}, R_{M-1,N-1}]^T$ denote the unknowns. For the boundary-point values, $V_{i,0}$, $V = S, I, R$, $i = 1, 2, \ldots, M-1$, we construct a cubic interpolation polynomial $P_3(y)$ of V at the grid points (x_i, y_0), (x_i, y_1), (x_i, y_2), and (x_i, y_3), and impose the no-flux boundary condition $P_3'(y_0) = 0$, which leads to

$$V_{i,0} = \frac{6}{11}(3V_{i,1} - \frac{3}{2}V_{i,2} + \frac{1}{3}V_{i,3}).$$

To discretize the Hamilton-Jacobi term using the third order WENO scheme, we need ghost point value $V_{i,-1}$. The extrapolation technique is used. Namely, we construct a cubic interpolation polynomial of V at (x_i, y_0), (x_i, y_1), (x_i, y_2) and (x_i, y_3), and evaluate it at (x_i, y_{-1}) with $V_{i,0}$ be replaced with the above equality, then we get

$$V_{i,-1} = \frac{1}{11}(6V_{i,1} + 8V_{i,2} - 3V_{i,3}).$$

Similarly, we obtain the values of S, I, R at the other boundary points.

Now we apply the second-order IIF (IIF2) temporal discretization. We use the approach in [11] to deal with the nonlinear diffusion terms in the SIR model. Spatial discretizations of Eq. 1 leads to the following semi-discretized ordinary differential equation (ODE) system

$$\frac{d\vec{U}}{dt} + \vec{H}(\vec{U}) = \vec{F}_d(\vec{U}) + \vec{F}_r(\vec{U}), \tag{4}$$

where $\vec{\tilde{H}}(\vec{U})$ and $\vec{F}_d(\vec{U})$ result from the spatial discretizations of the Hamilton-Jacobi term and the nonlinear diffusion terms respectively, and $\vec{F}_r(\vec{U})$ is the nonlinear reaction. Let $0 = t_0 < t_1 < \cdots < t_K = T$ be the partition in time. $\vec{U}_k \approx \vec{U}(t_k)$, and $C(\vec{U}_k) = \frac{\partial \vec{F}_d}{\partial \vec{U}}(\vec{U}_k)$ denotes the Jacobian matrix. We rewrite $\vec{F}_d(\vec{U})$ for $t \in [t_k, t_{k+1})$ as

$$\vec{F}_d(\vec{U}) = \vec{F}_d(\vec{U}_k) + C(\vec{U}_k)(\vec{U} - \vec{U}_k) + \vec{E}(\vec{U}), \tag{5}$$

where $\vec{E}(\vec{U})$ is the remainder. The Eq. 4 can be rewritten as

$$\frac{d\vec{U}}{dt} - C(\vec{U}_k)\vec{U} = \vec{F}_d(\vec{U}_k) - C(\vec{U}_k)\vec{U}_k + \vec{E}(\vec{U}) - \vec{\tilde{H}}(\vec{U}) + \vec{F}_r(\vec{U}). \tag{6}$$

Multiplying by $e^{-C(\vec{U}_k)t}$ and integrating Eq. 6 from $t = t_k$ to $t = t_{k+1}$, we get

$$\begin{aligned} \vec{U}_{k+1} \quad = \quad & e^{C_k\Delta t_k}\vec{U}_k + e^{C_k\Delta t_k}\int_0^{\Delta t_k} e^{-C_k\tau}(\vec{F}_d(\vec{U}(t_k+\tau)) - C_k\vec{U}(t_k+\tau) \\ & -\vec{\tilde{H}}(\vec{U}(t_k+\tau)) + \vec{F}_r(\vec{U}(t_k+\tau)))d\tau, \end{aligned} \tag{7}$$

where $C_k \triangleq C(\vec{U}_k)$ and $\Delta t_k = t_{k+1} - t_k$. The IIF schemes are obtained by approximating the integrand in Eq. 7 by Lagrange interpolation polynomials. See [11] for details. The second-order IIF scheme takes the following form:

$$\begin{aligned} \vec{U}_{k+1} \quad = \quad & e^{C_k\Delta t_k}\vec{U}_k + \Delta t_k\{\alpha_{k+1}\vec{F}_r(\vec{U}_{k+1}) + \alpha_k e^{C_k\Delta t_k}\vec{F}_r(\vec{U}_k) \\ & +\beta_{k-1}e^{C_k(\Delta t_k+\Delta t_{k-1})}(\vec{F}_d(\vec{U}_{k-1}) - C_k\vec{U}_{k-1} - \vec{\tilde{H}}(\vec{U}_{k-1})) \\ & +\beta_k e^{C_k\Delta t_k}(\vec{F}_d(\vec{U}_k) - C_k\vec{U}_k - \vec{\tilde{H}}(\vec{U}_k))\}, \end{aligned} \tag{8}$$

where $\alpha_k = \frac{1}{2}$, $\alpha_{k+1} = \frac{1}{2}$, $\beta_{k-1} = -\frac{\Delta t_k}{2\Delta t_{k-1}}$, and $\beta_k = \frac{1}{\Delta t_{k-1}}(\frac{\Delta t_k}{2} + \Delta t_{k-1})$.

Rewrite the second order scheme Eq. 8, we get

$$\begin{aligned} & \vec{U}_{k+1} - \Delta t_k\alpha_{k+1}\vec{F}_r(\vec{U}_{k+1}) \\ = \quad & e^{C_k\Delta t_k}\vec{U}_k + \Delta t_k\{\alpha_k e^{C_k\Delta t_k}\vec{F}_r(\vec{U}_k) + \beta_k e^{C_k\Delta t_k}(\vec{F}_d(\vec{U}_k) - C_k\vec{U}_k - \vec{\tilde{H}}(\vec{U}_k)) \\ & +\beta_{k-1}e^{C_k(\Delta t_k+\Delta t_{k-1})}(\vec{F}_d(\vec{U}_{k-1}) - C_k\vec{U}_{k-1} - \vec{\tilde{H}}(\vec{U}_{k-1}))\}. \end{aligned} \tag{9}$$

Denoting the right hand side terms as RHS, at each grid point (x_i, y_j) we have the following 3-equation nonlinear system

$$\begin{aligned} S_{i,j}^{k+1} - \Delta t_k\alpha_{k+1}\cdot(-\alpha S_{i,j}^{k+1}I_{i,j}^{k+1}) &= (RHS)_{i,j,S}, \\ I_{i,j}^{k+1} - \Delta t_k\alpha_{k+1}\cdot(\alpha S_{i,j}^{k+1}I_{i,j}^{k+1} - \gamma I_{i,j}^{k+1}) &= (RHS)_{i,j,I}, \\ R_{i,j}^{k+1} - \Delta t_k\alpha_{k+1}\cdot(\gamma I_{i,j}^{k+1}) &= (RHS)_{i,j,R}. \end{aligned}$$

Here $(RHS)_{i,j,S}$ corresponds to the component for $S_{i,j}$ in the right hand side vector of the Eq. 9, similarly for $(RHS)_{i,j,I}$ and $(RHS)_{i,j,R}$. It is worth to note that this is just a local nonlinear system with 3 equations for $S_{i,j}^{k+1}$, $I_{i,j}^{k+1}$, and $R_{i,j}^{k+1}$, for each pair of (i,j), $1 \le i \le M-1$, $1 \le j \le N-1$. Newton's method can be easily employed to solve the small nonlinear system. This shows an advantage of IIF schemes over many implicit schemes, namely, solving large coupled nonlinear algebraic system is avoided.

Evaluating of $e^{C_k\Delta t_k}\vec{v}$ is approximated by the Krylov subspace method for efficiently implementing IIF schemes to solve high spatial dimension problems [8]. The sparse matrix C_k is projected to the Krylov subspace

$$K_m = \text{span}\{\vec{v}, C_k\vec{v}, C_k^2\vec{v}, \ldots, C_k^{m-1}\vec{v}\}.$$

The well-known Arnoldi algorithm generates an orthonormal basis $V_m = [\vec{v}_1, \vec{v}_2, \ldots, \vec{v}_m]$ of the Krylov subspace K_m, and an $m \times m$ upper Hessenberg matrix H_m. That is $V_m^T C_k V_m = H_m$. Thus, we have the approximation

$$e^{C_k \Delta t_k} \vec{v} \approx \tilde{\gamma} V_m e^{H_m \Delta t_k} \vec{e}_1,$$

where $\tilde{\gamma} = \|\vec{v}\|_2$, and $\vec{e}_1$ denotes the first column of the $m \times m$ identity matrix I_m. In the paper, $m = 25$ is being used.

3. Order of convergence of the Krylov IIF WENO scheme.

3.1. **One-dimensional cases.** First we apply the proposed Krylov IIF WENO method to the following problem:

$$\begin{cases} S_t &= k_1(S(S_x + I_x + R_x))_x + k_2(SI_x)_x - \alpha SI + f_S(x,t), \\ I_t &= k_1(S(S_x + I_x + R_x))_x + \alpha SI - \gamma I + f_I(x,t), \quad (x,t) \in \Omega_T, \\ R_t &= k_1(S(S_x + I_x + R_x))_x + \gamma I + f_R(x,t), \end{cases} \tag{10}$$

where $\Omega = (0, \pi)$, $\Omega_T = \Omega \times (0, T)$, f_S, f_I, and f_R are chosen so that the system has a solution

$$S(x,t) = e^{-t}(1 - \cos(2x)),\ I(x,t) = e^{-t}(1 + \cos(x)),\ R(x,t) = e^{-t}(1 - \cos(x)).$$

The initial condition of the system is set by using the true solution with $t = 0$. The system is subject to no-flux boundary conditions. Throughout this paper, we take $\alpha = 1$ and $\gamma = 5$. We set $T = 1$ for all the simulations in this section. One advantage of the Krylov IIF WENO scheme for solving the fully nonlinear Hamilton-Jacobi-diffusion-reaction system is that the time step size Δt_k can be adaptively chosen as that for a pure hyperbolic PDE. The time step size Δt_k satisfies the following Courant-Friedrichs-Lewy (CFL) condition for the two-dimensional problem

$$\Delta t_k(\alpha_x \frac{1}{\Delta x} + \alpha_y \frac{1}{\Delta y}) = \text{CFL},$$

where CFL is a specified number, called the CFL number. α_x and α_y are defined in the Eq. 3. At every time step, α_x and α_y are updated using the Eq. 3, then the time step size Δt_k is determined by the above CFL condition. Δt_k will be used to evolve the numerical solution to the next time step. In one-dimensional case, the above equality is reduced into $\Delta t_k \alpha_x \frac{1}{\Delta x} = \text{CFL}$. This indicates the high efficiency of the Krylov IIF WENO scheme for solving the problems with diffusion terms, i.e., large time step size computations ($\Delta t = O(\Delta x)$) are achieved.

3.1.1. *Case 1:* $k_1 = 0.1$ *and* $k_2 = 0.001$. As shown in [12], the Eq. 10 is ill-posed for its long-term behavior. To start the computation by the Krylov IIF2 WENO scheme, the numerical values at the first and the second time steps, i.e., $\vec{U}_0$ and $\vec{U}_1$ are needed. $\vec{U}_0$ can be directly computed by using the initial condition of the PDE. Here for simplicity, $\vec{U}_1$ is set by using the exact solution. For the problems with unknown exact solutions, $\vec{U}_1$ is computed by using a second order Runge-Kutta method. The numerical solutions are obtained for Eq. 10 at $T = 1$. The CFL number is taken to be 0.2. Numerical results are reported in Table 1. From Table 1, it is clear that the desired second-order accuracy is obtained for the proposed Krylov IIF2 WENO scheme. It is worthy to note that if $\vec{U}_1$ is computed with a second order Runge-Kutta method, a similar table with the same order of accuracy can be acquired.

N	L^∞ error	L^∞ order	L^1 error	L^1 order	L^2 error	L^2 order
10	3.85e-02	-	7.48e-03	-	1.07e-02	-
20	1.24e-02	1.64	2.28e-03	1.72	3.53e-03	1.60
40	3.29e-03	1.91	5.56e-04	2.03	8.95e-04	1.98
80	8.30e-04	1.99	1.45e-04	1.94	2.26e-04	1.98
160	2.07e-04	2.00	3.68e-05	1.98	5.67e-05	2.00
320	5.12e-05	2.01	9.21e-06	2.00	1.42e-05	2.00

TABLE 1. Numerical results of the one-dimensional system Eq. 10 for $k_1 = 0.1$ and $k_2 = 0.001$. π/N is the mesh size in the spatial direction. Here the constant CFL $= 0.2$.

3.1.2. *Case 2:* $k_1 = 0.1$ *and* $k_2 = 0$. In this case, the coefficient matrix of the second-order terms at the right hand side of Eq. 10 has two zero eigenvalues and one positive eigenvalue. The nonlinear term of Eq. 10 behaves like a porous media equation. We expect that for this well-posed case, the CFL number can take larger values than in the previous case. In addition, Table 2 shows the numerical results for CFL $= 0.2$ and Table 3 shows the numerical results for CFL $= 0.5$. It can be seen that both tables demonstrate the desired second order accuracy, while a smaller CFL number results in smaller numerical errors. Again, the time step size $\Delta t = O(\Delta x)$ shows that the Krylov IIF WENO scheme is an efficient numerical method for this type of problems which involve diffusion terms.

N	L^∞ error	L^∞ order	L^1 error	L^1 order	L^2 error	L^2 order
10	3.86e-02	-	7.51e-03	-	1.07e-02	-
20	1.24e-02	1.63	2.29e-03	1.72	3.54e-03	1.60
40	3.30e-03	1.91	5.59e-04	2.03	9.00e-04	1.98
80	8.31e-04	1.99	1.45e-04	1.95	2.27e-04	1.98
160	2.07e-04	2.00	3.69e-05	1.97	5.70e-05	2.00
320	5.15e-05	2.01	9.29e-06	1.99	1.43e-05	2.00

TABLE 2. Numerical results of the one-dimensional system Eq. 10 for $k_1 = 0.1$ and $k_2 = 0$. CFL $= 0.2$. π/N is the mesh size in the spatial direction.

N	L^∞ error	L^∞ order	L^1 error	L^1 order	L^2 error	L^2 order
10	1.05e-01	-	3.23e-02	-	4.05e-02	-
20	4.17e-02	1.33	8.41e-03	1.94	1.27e-02	1.67
40	1.46e-02	1.51	2.69e-03	1.65	4.04e-03	1.65
80	3.94e-03	1.89	7.25e-04	1.89	1.10e-03	1.88
160	1.05e-03	1.91	1.94e-04	1.91	2.91e-04	1.92
320	2.61e-04	2.00	4.96e-05	1.96	7.35e-05	1.99

TABLE 3. Numerical results of the one-dimensional system Eq. 10 for $k_1 = 0.1$ and $k_2 = 0$. CFL $= 0.5$. π/N is the mesh size in the spatial direction.

3.1.3. *Case 3:* $k_1 = 0$, $k_2 = 0.1$. When $k_1 = 0$, and $k_2 > 0$, the last two equations are reduced into ordinary differential equations. The proposed Krylov IIF2 WENO scheme can be still directly applied to this degenerate case. Table 4 shows the numerical results for this special case. The CFL number is taken to be 0.1. Again, we can see that the Krylov IIF2 WENO scheme has reached the desired second-order accuracy, with large time step size $\Delta t = O(\Delta x)$.

N	L^∞ error	L^∞ order	L^1 error	L^1 order	L^2 error	L^2 order
10	3.38e-02	-	5.95e-03	-	7.33e-03	-
20	1.05e-02	1.68	1.88e-03	1.66	2.27e-03	1.69
40	2.92e-03	1.85	5.53e-04	1.77	6.64e-04	1.78
80	7.93e-04	1.88	1.53e-04	1.85	1.80e-04	1.88
160	2.08e-04	1.93	4.03e-05	1.92	4.71e-05	1.94
320	5.35e-05	1.96	1.04e-05	1.95	1.21e-05	1.96

TABLE 4. Numerical results of the one-dimensional system Eq. 10 for $k_1 = 0$ and $k_2 = 0.1$. CFL $= 0.1$. π/N is the mesh size in the spatial direction.

3.2. **Two-dimensional cases.** In this section, we apply the Krylov IIF WENO method to the following two-dimensional problem:

$$\begin{cases} S_t &= k_1(S(S_x + I_x + R_x))_x + k_2(SI_x)_x + k_1(S(S_y + I_y + R_y))_y + k_2(SI_y)_y \\ & \quad -\alpha SI + f_S(x,y,t), \\ I_t &= k_1(I(S_x + I_x + R_x))_x + k_1(I(S_y + I_y + R_y))_y + \alpha SI - \gamma I + f_I(x,y,t), \\ R_t &= k_1(R(S_x + I_x + R_x))_x + k_1(R(S_y + I_y + R_y))_y + \gamma I + f_R(x,y,t). \end{cases} \tag{11}$$

This system is defined on the spatial domain $(0,\pi) \times (0,\pi)$. f_S, f_I, and f_R are chosen so that the system has a solution

$$S(x,y,t) = e^{-t}(1-\cos(2x))(1-\cos(2y)),\ I(x,y,t) = e^{-t}(1+\cos(x))(1+\cos(y)),$$
$$R(x,y,t) = e^{-t}(1-\cos(x))(1-\cos(y)).$$

The initial condition of the system is set by using the true solution with $t = 0$. The system is subject to no-flux boundary conditions. The parameters $\alpha = 1$ and $\gamma = 5$. Again for simplicity, $\vec{U}_1$ is set by using the exact solution. Of course, a second-order Runge-Kutta method can also be used to compute $\vec{U}_1$ to start the time evolution. We run the simulation till time $T = 1$ by the Krylov IIF2 WENO scheme. Table 5 shows the numerical results for the case where $k_1 = 0.1$ and $k_2 = 0.001$. The numerical results for the case where $k_1 = 0.1$ and $k_2 = 0$ are reported in Table 6, and those for the case where $k_1 = 0$ and $k_2 = 0.1$ are given in Table 7. We draw the same conclusion as that for the one-dimensional system. The proposed Krylov IIF2 WENO method reaches the desired second-order accuracy for solving the two-dimensional system Eq 11. Large time step size $\Delta t = O(\Delta x)$ is achieved by using the efficient Krylov IIF2 WENO scheme to solve this system.

Remark. We have demonstrated that the proposed Krylov IIF2 WENO method has desired second-order accuracy for solving the model systems Eq. 10 and Eq. 11. The method works very well for different cases where k_1 and k_2 take various values. In our numerical experiments, we also observe that the numerical method may suffer instability for some strongly ill-posed cases such as $k_1 = 0.1$ and $k_2 = 0.1$. In these

N	L^∞ error	L^∞ order	L^1 error	L^1 order	L^2 error	L^2 order
10	6.21e-02	-	7.34e-03	-	9.75e-03	-
20	1.73e-02	1.84	1.65e-03	2.15	2.39e-03	2.03
40	2.69e-03	2.69	4.01e-04	2.04	6.37e-04	1.91
80	5.99e-04	2.16	9.09e-05	2.14	1.45e-04	2.13
160	1.39e-04	2.10	2.15e-05	2.08	3.43e-05	2.08
320	3.35e-05	2.05	5.18e-06	2.06	8.25e-06	2.06

TABLE 5. Numerical results of the two-dimensional system Eq. 11 for $k_1 = 0.1$ and $k_2 = 0.001$. CFL $= 0.4$. π/N is the mesh size in each of the spatial directions.

N	L^∞ error	L^∞ order	L^1 error	L^1 order	L^2 error	L^2 order
10	7.30e-02	-	1.02e-02	-	1.32e-02	-
20	2.12e-02	1.78	2.54e-03	2.00	3.76e-03	1.82
40	4.15e-03	2.35	6.54e-04	1.96	1.03e-03	1.88
80	1.03e-03	2.01	1.56e-04	2.07	2.47e-04	2.05
160	2.77e-04	1.90	3.86e-05	2.02	6.05e-05	2.03
320	6.97e-05	1.99	7.92e-06	2.28	1.28e-05	2.25

TABLE 6. Numerical results of the two-dimensional system Eq. 11 for $k_1 = 0.1$ and $k_2 = 0$. CFL $= 0.6$. π/N is the mesh size in each of the spatial directions.

N	L^∞ error	L^∞ order	L^1 error	L^1 order	L^2 error	L^2 order
10	3.08e-02	-	2.91e-03	-	3.72e-03	-
20	7.74e-03	1.99	8.37e-04	1.80	1.17e-03	1.67
40	1.68e-03	2.20	2.37e-04	1.82	3.32e-04	1.82
80	4.18e-04	2.01	6.24e-05	1.93	8.68e-05	1.94
160	1.07e-04	1.97	1.64e-05	1.93	2.24e-05	1.96
320	2.69e-05	1.99	4.13e-06	1.98	5.65e-06	1.99

TABLE 7. Numerical results of the two-dimensional system Eq. 11 for $k_1 = 0$ and $k_2 = 0.1$. CFL $= 0.2$. π/N is the mesh size in each of the spatial directions.

strongly ill-posed cases, the coefficient matrix of the second order term has one relatively large negative eigenvalue, which gives a strongly backward heat equation component in the system. This may cause instability for the numerical method, especially in refined meshes. How to deal with these most difficult cases is one of our next research topics.

4. **Application of the Krylov IIF WENO method to the SIR model.** In this section, we apply the Krylov IIF2 WENO method to the SIR model with directed diffusion, i.e., the system Eq. 1. Two biologically interesting cases are studied: (i) $k_1 = 0$, $k_2 > 0$, corresponding to the directed dispersion avoiding infection; (ii) $k_1 > 0$, $k_2 = 0$, corresponding to the directed dispersion avoiding crowding.

4.1. **Case 1: $k_1 = 0$, $k_2 > 0$ (avoiding infection).** First let us consider the same example as in the Milner and Zhao's paper [18] for the one-dimensional case where $k_2 = 0.1$, $\alpha = 1$, and $\gamma = 5$. Let $\Omega = (0, 1)$. The initial condition are chosen as $S_0(x) = 6$, $R_0(x) = 0$, for $x \in \Omega$ and

$$I_0(x) = \begin{cases} 2 - 25x^2, & 0 \le x \le 0.1, \\ \frac{25}{7}(0.8 - x)^2, & 0.1 < x \le 0.8, \\ 0 & 0.8 < x \le 1. \end{cases} \tag{12}$$

The solution might break down with a formation of a shock wave, or a finite-time blow-up solution might exist by rewriting the system as a hyperbolic system [16]. The discontinuity occurs on the boundary of compact support of infected individuals, $x = 0.8$. Numerical simulations in [18] suggest that there might exist a finite-time blow-up solution at $t = 0.7$. Following the approach in [18], we compute the numerical solutions of S at $t = 0.7$ and at mesh points $x = 0.8 - \frac{1}{M}$, $M = 1280, 640, \ldots, 10$. Then, we compute the ratio $r = S(0.8 - \frac{1}{M})/S(0.8 - \frac{1}{M/2})$. If r approaches a constant, we can conjecture that S takes the form $S(x) = \dfrac{\text{const}}{(0.8 - x)^\alpha}$ where $\alpha = \ln(r)/ln(2)$. Table 8 shows the numerical results using the Krylov IIF WENO scheme for the system with the above initial condition. We can see that the value of r still has a little oscillation at $t = 0.7$ when M approaches 1280. The convergence of r has a better pattern at $t = 0.706$, as shown in Table 8. This indicates that the solution might blow-up at $t = 0.706$ instead of $t = 0.7$. Figure 1 shows the density profile of solutions of Eq. 1 at $t = 0.706$. We can see that the singularity of the solution has been resolved well by the Krylov IIF WENO scheme.

M	10	20	40	80	160	320	640	1280
S (at T = 0.7)	7.05	9.72	13.39	18.49	25.56	36.15	66.84	80.74
r (at T = 0.7)	-	1.37	1.38	1.38	1.38	1.41	1.85	1.21
S (at T = 0.706)	6.97	9.56	13.09	17.88	24.31	33.71	54.05	89.15
r (at T = 0.706)	-	1.37	1.37	1.37	1.36	1.39	1.60	1.65

TABLE 8. Numerical solution of S at $t = 0.7$ and $t = 0.706$ and $x = 0.8 - 1/M$ for different M. All values are computed using the uniform mesh $\Delta x = 1/1280$.

Numerically verifying the finite-time blow-up is challenging. Hirota et al proposed a numerical method to estimate the blow-up time for the problems of partial differential equations [10]. However, the method was applied to the test problems where the partial differential equation does have finite-time blow-up solutions. We conjecture that susceptibles might be finite-time blow-up at $x = 0.8$, the compact support boundary of the infective individuals, at time $t = 0.706$. On the other hand, if we do not assume that there is a finite-time blow-up solution, we will expect that a form of shock or discontinuity of solutions occurs. As infected individuals can not move away from their compact support region, susceptibles will stop moving further as soon as they reach a safe zone of infection free region. This will result to a situation where the population accumulation of susceptibles on the boundary of compact support of infected individuals. Numerical simulation shows the discontinuity of solution, particularly in I. Figure 2 shows the numerical solution of the

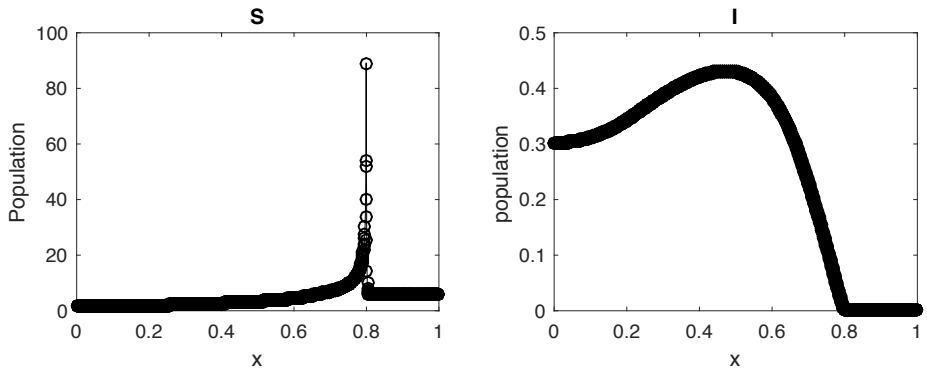

FIGURE 1. Numerical solution of the one-dimensional case of Eq. 1 for the case of avoiding infection ($k_1 = 0$ and $k_2 = 0.1$) at $t = 0.706$. CFL $= 0.1$.

one-dimensional case of Eq. 1 at $t = 1.5$. We can see that the discontinuities of the solution are resolved very well, even with a relatively coarse mesh $N = 40$. The WENO approximation plays a key role here in capturing the discontinuities of the solution sharply and stably.

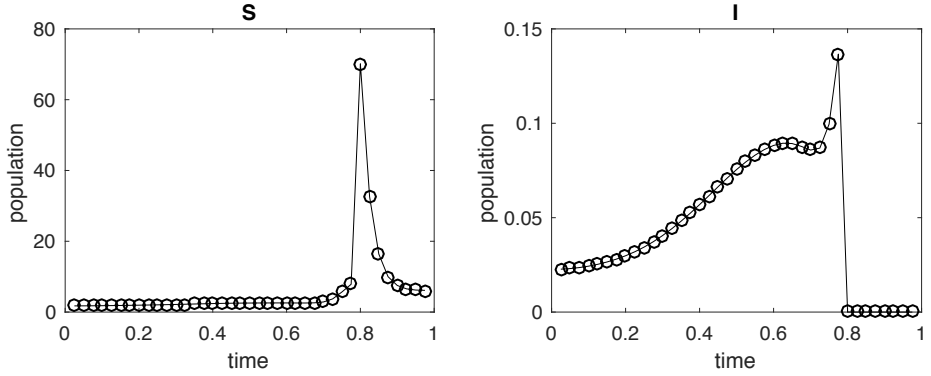

FIGURE 2. Numerical solution of the one-dimensional case of Eq. 1 for the case of avoiding infection ($k_1 = 0$, $k_2 = 0.1$) at $t = 1.5$. CFL $= 0.1$.

In the two-dimensional case, Milner and Zhao [18] also conjectured that a finite-time blow-up solution might exist. Let $\Omega = (0, 1) \times (0, 1)$, $S_0(x, y) = 6$, $R_0(x, y) = 0$ on Ω, and $I(x, y)$ is the tensor product of the function in Eq. 12. Again, we take the parameter values $k_1 = 0$ and $k_2 = 0.1$. Figure 3 shows the numerical solution of Eq. 1 for the two-dimensional case with the above initial conditions. From the figure, it is reasonable to believe that the finite-time blow-up solution occurs first at the intersection of domain boundary and the boundary of compact support of initial conditions of infected individuals. As that for the one-dimensional case, the singularities of the solution have been resolved very well by the Krylov IIF

WENO scheme. In [18], it was observed that the finite-time blow-up might occur along the boundary of the initial compact of infected individuals. We believe that the higher-order numerical scheme in this paper can better capture the behavior of finite-time blow-up of solutions. Similarly as in the one-dimensional case, the numerical scheme in this paper allows us to run the simulation beyond $t = 0.7$. We observe accumulation of susceptibles on the boundary of compact support of initial infected population as t increases.

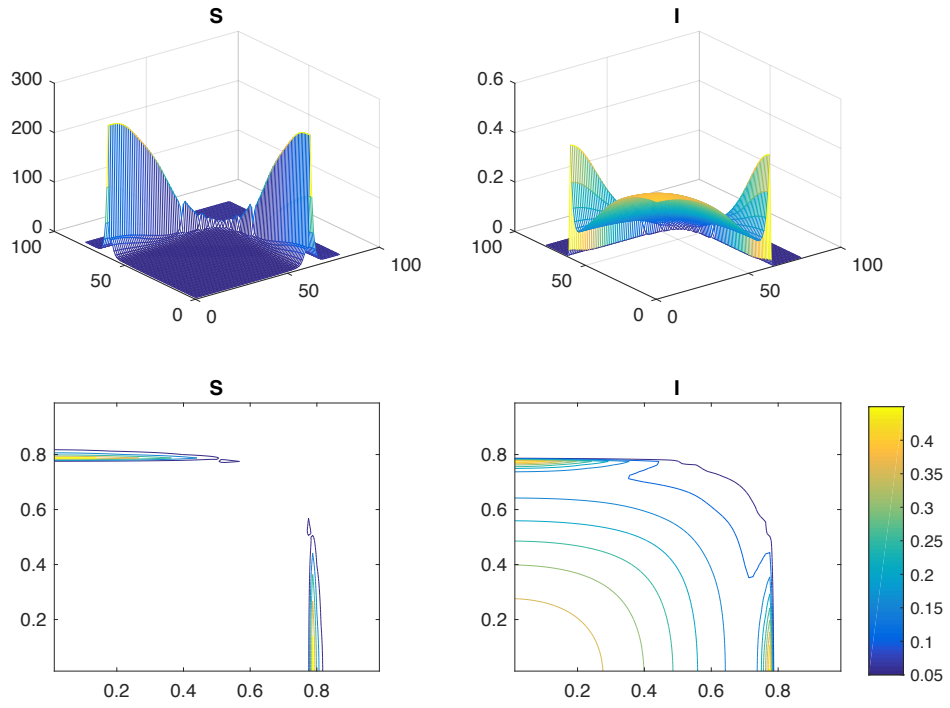

FIGURE 3. Numerical solution of the two-dimensional case of Eq. 1 for the case of avoiding infection ($k_1 = 0$, $k_2 = 0.1$) at $t = 0.7$. CFL $= 0.2$.

4.2. **Case 2: $k_1 > 0$, and $k_2 = 0$ (avoiding crowd).** Here we consider the case corresponding to the directed dispersion avoiding crowding. Besides S, I and R, we also study the dynamics of total population $P = S + I + R$. Notice that by adding three equations of Eq. 1, the total population actually satisfies a porous media equation

$$\frac{dP}{dt} = k_1 \nabla \dot{(} P \nabla P). \tag{13}$$

It is clear that the Krylov IIF WENO scheme can be directly applied to the Eq. 13 if we are only interested in the dynamics of total population. Here we still solve the original system Eq. 1 to find S, I and R by the Krylov IIF WENO method. The total population P is evaluated by adding S, I and R we obtain.

In the one-dimensional case, we use the same initial condition as that in the previous section. The parameter values are set as $k_1 = 0.1$ and $k_2 = 0$. At the

steady-state, the infected individuals will vanish and the total population will approach a constant. This is verified by our numerical simulation. Figure 4 shows the density profiles of populations at $t = 0$ and at $t = 20$, respectively. At $t = 20$, the numerical solution reaches the steady-state. In this case, the CFL number can be taken as large as 0.6.

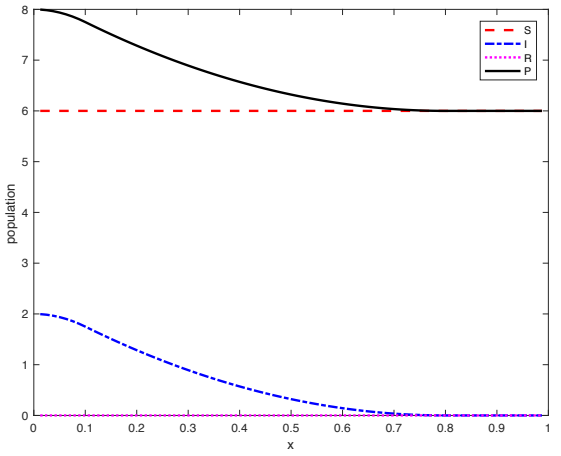

a. $T = 0$

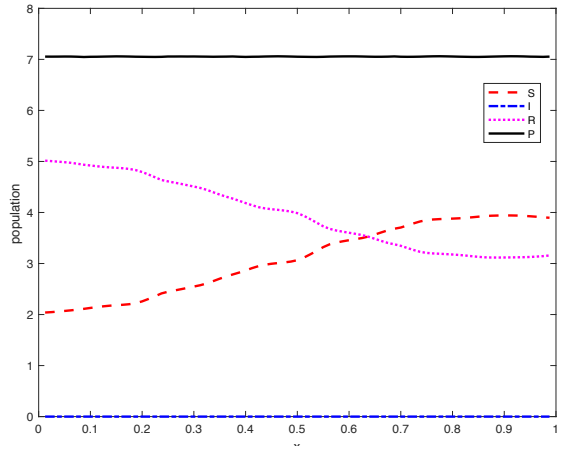

b. $T = 20$

FIGURE 4. Numerical solution for the one-dimensional case of Eq. 1 for avoiding crowd ($k_1 = 0.1$, $k_2 = 0$). CFL = 0.6.

In the two-dimensional case, we use the tensor product of the initial condition in the one-dimensional case. We take CFL = 0.2. Figure 5 shows the initial density of populations. The numerical solutions of Eq. 1 at $t = 1$, $t = 10$ and $t = 25$ are shown in Figure 6, Figure 7 and Figure 8, respectively. From the figures, we see that the total population P approaches a constant; the infected individuals vanish; and the susceptible and recovered individuals converge to their own steady-states. This observation is consistent with that in the one-dimensional case.

5. **Conclusion and discussions.** Mathematical models with directed diffusions are important in describing the population movement. In particular, the population

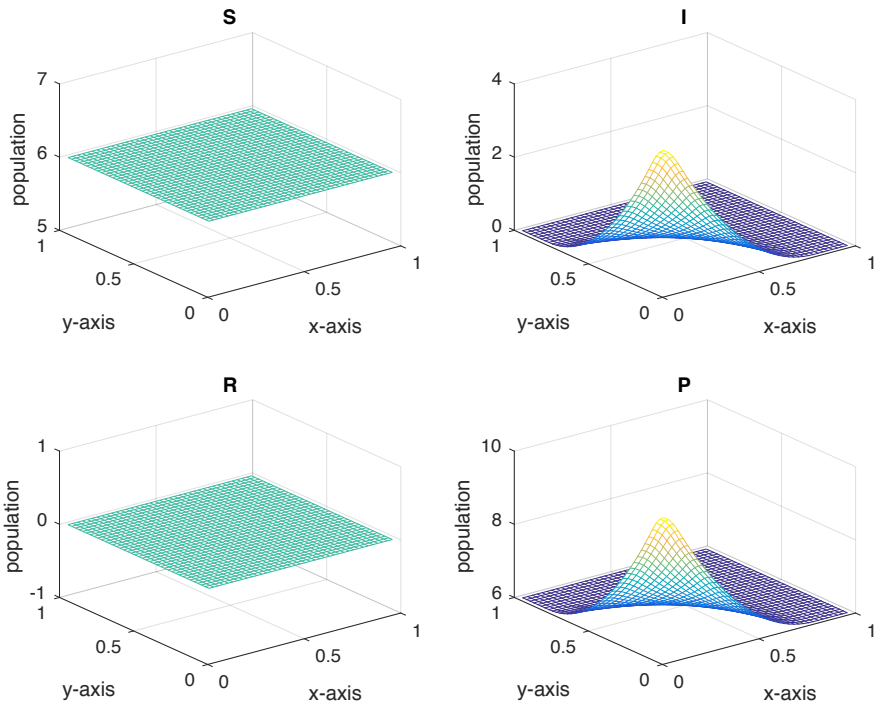

FIGURE 5. Initial density profiles of population at $t = 0$.

will move away from crowd and also away from infection during epidemics. However, such models are usually difficult to simulate since the describing system of partial differential equations is often degenerated or sometimes even not well-posed. For example, the leading coefficient matrix of Eq. 1 might have one positive eigenvalue, one negative eigenvalue and one zero eigenvalue when $k_1 > 0$ and $k_2 > 0$. Therefore, the system might behave as a mixture of heat equation, backward heat equation, and hyperbolic system. Numerically simulating such models is often very challenging.

In this paper, we design a Krylov implicit integration factor WENO method to solve the SIR models with directed diffusions. The method is demonstrated to have second-order accuracy by using test problems with smooth solutions, for the general case ($k_1 > 0$ and $k_2 > 0$) and two biologically interesting cases: (i) avoid infection ($k_1 = 0$, $k_2 > 0$) and (ii) avoid crowd ($k_1 > 0$ and $k_2 = 0$). Numerical simulations show the high efficiency of the Krylov IIF WENO method in solving the SIR models with directed diffusion. Singularities in the solution are resolved stably and sharply by the WENO approximations in the scheme. Unlike a usual implicit method for solving stiff nonlinear PDEs, the Krylov IIF WENO method avoids solving large coupled nonlinear algebraic systems at every time step. Only a system of three nonlinear equations need to be solved at every grid point for the SIR model in this paper. These small nonlinear systems can be solved easily by the Newton's method. Large time step size computations are achieved, namely, the time step size $\Delta t = O(\Delta x)$ for solving the fully nonlinear second-order PDEs in

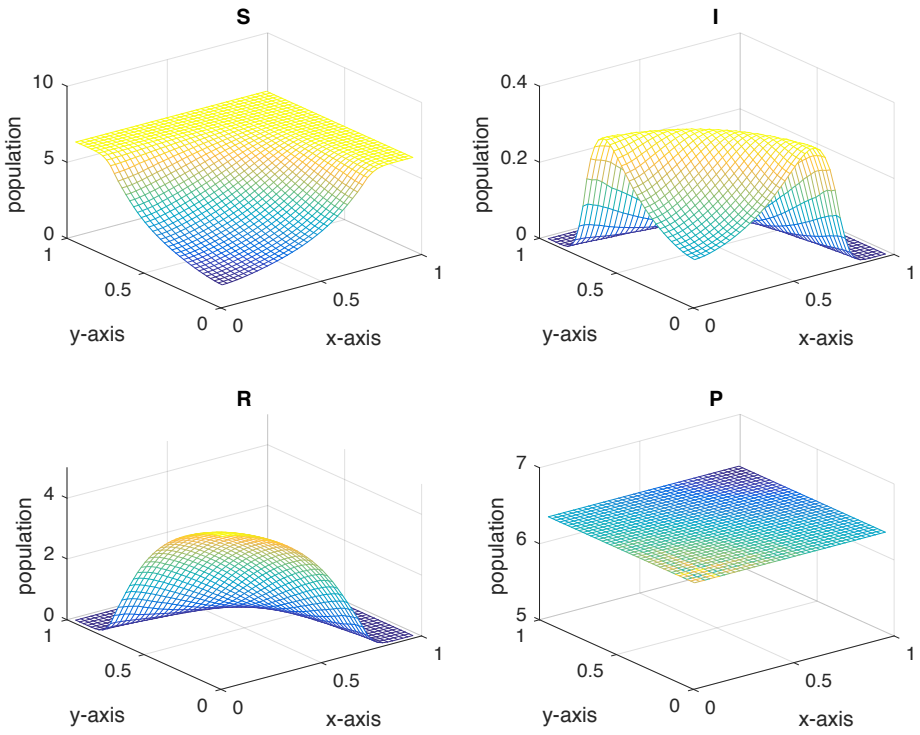

FIGURE 6. Numerical solution of the two-dimensional case of Eq. 1 for avoiding crowd ($k_1 = 0.1$, $k_2 = 0$) at $t = 1$. CFL $= 0.2$.

this paper. The time step size Δt is adaptively determined at every time step by the CFL condition as that for a pure hyperbolic PDE.

The numerical results of the Krylov IIF WENO method applied to Eq. 1 show the consistent results as that obtained in [18]. Furthermore, it suggests that the finite-time blow-up might occur on the special points in the spatial domain rather than along a curve for the two-dimensional case. High order numerical methods are important in capturing the details of the system, such as finding the finite-time blow-up time and location or discontinuity locations in this case.

Mathematical modeling population's spatial movement is biologically important. Other cross-diffusion models were studied in the literatures (see the introduction). High order numerical methods will be efficient to simulate such models. A possible future work is to apply the Krylov IIF WENO scheme to other cross-diffusion mathematical models. Human spatial movement typically happens in two dimensions. The proposed Krylov IIF WENO scheme can be easily applied to three dimensional applications, such as fish movement in the contaminated water system. The spatial discretizations are based on finite difference schemes, hence dimension-by-dimension approach can be directly applied to multidimensional problems (e.g., three dimensional problems). Although for three dimensional problems or even higher dimensional problems, we will obtain a ODE system with much larger size than that for two dimensional problems, the Krylov IIF scheme can still solve the

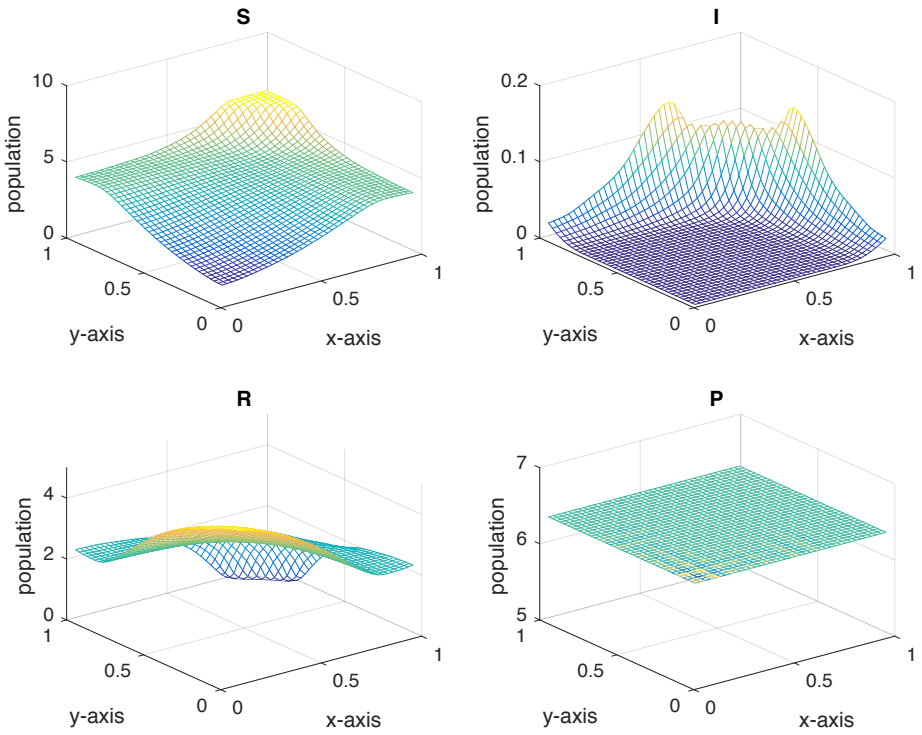

FIGURE 7. Numerical solution of the two-dimensional case of Eq. 1 for avoiding crowd ($k_1 = 0.1$, $k_2 = 0$) at $t = 10$. CFL $= 0.2$.

system efficiently, as that shown in [14]. For problems with other boundary conditions, corresponding algebraic equations can be derived for the boundary points based on that specific boundary condition. Then the derived algebraic equations will be used to form the ODEs for grid points adjacent to the boundary points. Hence we will obtain a slightly different ODE system, which can be solved directly by the proposed Krylov IIF scheme.

Acknowledgments. The first author (R. Zhao) would like to thank Dr. Fabio Milner for valuable discussions. Research of the second author (Y.-T. Zhang) is supported by NSF grant DMS-1620108. The authors also like to thank the anonymous reviewers for valuable comments to improve the manuscript.

REFERENCES

[1] L. Allen, B. Bolker, Y. Lou and A. Nevai, Asymptotic profiles of the steady states for an SIS epidemic reaction-diffusion model, *Discrete and Continuous Dynamical Systems Series B*, **21** (2008), 1–20.

[2] S. Berres and R. Ruiz-Baier, A fully adaptive numerical approximation for a two-dimensional epidemic model with nonlinear cross-diffusion, *Nonlinear Analysis: Real World Applications*, **12** (2011), 2888–2903.

[3] M. Bertsch and M. E. Gurtin, On predator-prey dispersal, repulsive dispersal, and the presence of shock waves, *Quarterly of Applied Mathematics*, **44** (1986), 339–351.

[4] M. Bertsch, M. E. Gurtin, D. Hilhorst and L. Peletier, On interacting populations that disperse to avoid crowding: Preservation of segregation, *J. Math. Biology*, **23** (1985), 1–13.

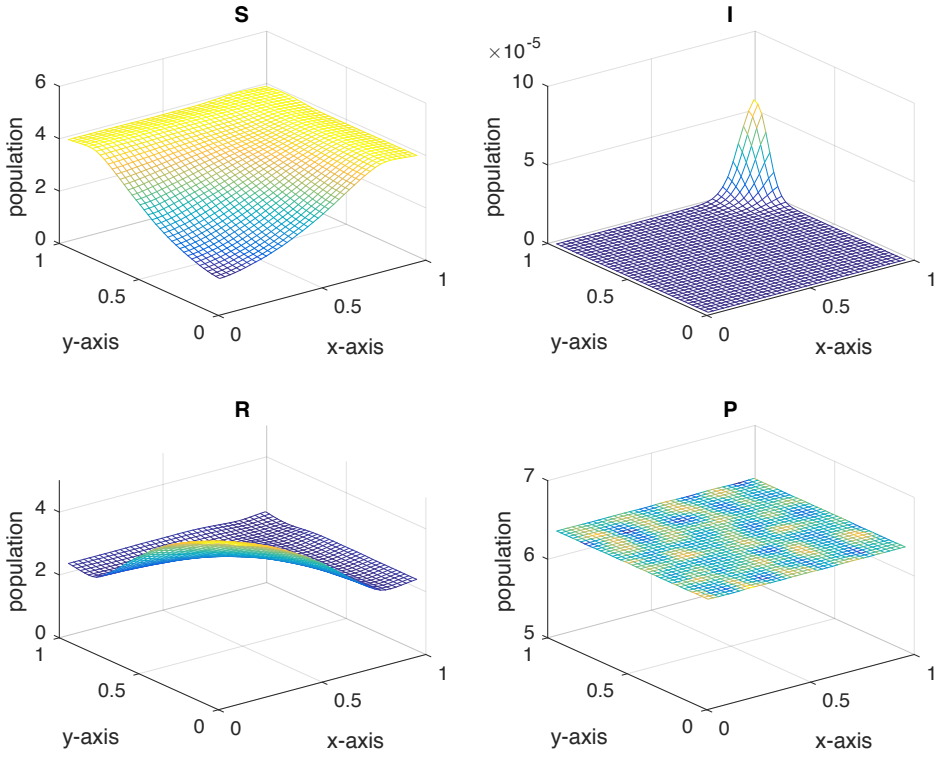

FIGURE 8. Numerical solution of the two-dimensional case of Eq. 1 for avoiding crowd ($k_1 = 0.1$, $k_2 = 0$) at $t = 25$. CFL $= 0.2$.

[5] M. Bertsch, M. E. Gurtin, D. Hilhorst and L. A. Peletier, On interacting populations that disperse to avoid crowding: The effect of a sedentary colony, *Journal of Mathematical Biology*, **19** (1984), 1–12.

[6] E. A. Carl, Population control in arctic ground squirrels, *Ecology*, **52** (1971), 395–413.

[7] L. Chang and Z. Jin, Efficient numerical methods for spatially extended population and epidemic models with time delay, *Applied Mathematics and Computation*, **316** (2018), 138–154.

[8] S. Chen and Y.-T. Zhang, Krylov implicit integration factor methods for spatial discretization on high dimensional unstructured meshes: application to discontinuous Galerkin methods, *Journal of Computational Physics*, **230** (2011), 4336–4352.

[9] M. E. Gurtin and R. C. MacCamy, On the diffusion of biological populations, *Mathematical Biosciences*, **33** (1977), 35–49.

[10] C. Hirota and K. Ozawa, Numerical method of estimating the blow-up time and rate of the solution of ordinary differential equations—an application to the blow-up problems of partial differential equations, *Journal of Computational and Applied Mathematics*, **193** (2006), 614–637.

[11] T. Jiang and Y.-T. Zhang, Krylov implicit integration factor WENO methods for semi-linear and fully nonlinear advection-diffusion-reaction equations, *Journal of Computational Physics*, **253** (2013), 368–388.

[12] F. Li and N. K. Yip, Long time behavior of some epidemic models, *Discrete and Continuous Dynamical Systems Series B*, **16** (2011), 867–881.

[13] D. Lu and Y.-T. Zhang, Krylov integration factor method on sparse grids for high spatial dimension convection-diffusion equations, *Journal of Scientific Computing*, **69** (2016), 736–763.

[14] D. Lu and Y.-T. Zhang, Computational complexity study on Krylov integration factor WENO method for high spatial dimension convection-diffusion problems, *Journal of Scientific Computing*, **73** (2017), 980–1027.
[15] R. C. MacCamy, Simple population models with diffusion, *Comp. & Maths with Appls*, **9** (1983), 341–344.
[16] D. B. Meade and F. A. Milner, An S-I-R model for epidemics with diffusion to avoid infection and overcrowding, *Proceedings of the 13th IMACS World Congress on Computation and Applied Mathematics*, **3** (1991), 1444–1445.
[17] D. B. Meade and F. A. Milner, S-I-R epidemic models with directed diffusion. In G. D. Prato, editor, Mathematical Aspects of Human Diseases, 1992.
[18] F. A. Milner and R. Zhao, S-I-R model with directed spatial diffusion, *Mathematical Population Studies*, **15** (2008), 160–181.
[19] Q. Nie, Y.-T. Zhang and R. Zhao, Efficient semi-implicit schemes for stiff systems, *Journal of Computational Physics*, **214** (2006), 521–537.
[20] Q. Nie, F. Wan, Y.-T. Zhang and X.-F. Liu, Compact integration factor methods in high spatial dimensions, *Journal of Computational Physics*, **227** (2008), 5238–5255.
[21] S. Osher and C.-W. Shu, High-order essentially nonoscillatory schemes for Hamilton-Jacobi equations, *SIAM J. Numer. Anal.*, **28** (1991), 907–922.
[22] N. Shigesada, K. Kawasaki and E. Teramoto, Spatial segregation of interacting species, *J. Theor. Biol.*, **79** (1979), 83–99.
[23] C.-W. Shu, Essentially non-oscillatory and weighted essentially non-oscillatory schemes for hyperbolic conservation laws, in *Advanced Numerical Approximation of Nonlinear Hyperbolic Equations*, B. Cockburn, C. Johnson, C.-W. Shu and E. Tadmor (Editor: A. Quarteroni), Lecture Notes in Mathematics, volume 1697, Springer, 1998, 325–432.
[24] J. G. Skellam, Random dispersal in theoretical populations, *Biometrika.*, **38** (1981), 196–218.
[25] G.-Q. Sun, Z. Jin, Q.-X. Liu and L. Li, Spatial pattern in an epidemic system with cross-diffusion of the susceptible, *Journal of Biological Systems*, **17** (2009), 141–152.
[26] D. Wang, W. Chen and Q. Nie, Semi-implicit integration factor methods on sparse grids for high-dimensional systems, *Journal of Computational Physics*, **292** (2015), 43–55.
[27] G. F. Webb, A reaction-diffusion model for a deterministic diffusion epidemic, *J. Math. Anal. Appl.*, **84** (1981), 150–161.
[28] K. E. Yong, E. D. Herrera, and C. Castillo-Chavez, From bee species aggregation to models of disease avoidance: The ben-hur effect. *Mathematical and Statistical Modeling for Emerging and Re-emerging Infectious Diseases*, **12** (2016), 169–185.
[29] Y.-T. Zhang and C.-W. Shu, High order WENO schemes for Hamilton-Jacobi equations on triangular meshes, *SIAM Journal on Scientific Computing*, **24** (2003), 1005–1030.
[30] Y.-T. Zhang and C.-W. Shu, ENO and WENO schemes, in *Handbook of Numerical Analysis*, Volume 17, Handbook of Numerical Methods for Hyperbolic Problems: Basic and Fundamental Issues, R. Abgrall and C.-W. Shu, Editors, North-Holland, Elsevier, Amsterdam, (2016), 103–122.
[31] Y.-T. Zhang, H.-K. Zhao and J. Qian, High order fast sweeping methods for static Hamilton-Jacobi equations, *Journal of Scientific Computing*, **29** (2006), 25–56.

Received June 2018; revised September 2018.

E-mail address: ruijun.zhao@mnsu.edu
E-mail address: yzhang10@nd.edu
E-mail address: chen39@iusb.edu